

Example 1: Holding Audience Attention with Dense Slides

Version #1

What is the data?

1840 A. R. MARSTON: RINGS AROUND WR STARS

WR star*	HD Number	Date observed	Filter	Exposure (secs)	Figure
WR16	HD86161	16 May 1994	H α	1800	2
WR30	HD94305	15 May 1994	H α	900	3a
WR30	-	19 May 1994	[O III]	2100	3b
WR40	HD96548	18 May 1994	H α	1800	4a
WR40	-	19 May 1994	[O III]	2100	4b
WR75	HD14749	17 May 1994	H α	2700	1a
WR75	-	17 May 1994	[O III]	2700	1b
WR85	HD8392B	16 May 1994	H α	900	5

* uses the nomenclature of van der Hucht et al. (1981).

ejection events. This uses a similar line of argument to that proposed by Balick et al. (1992) for using the extended halos of planetary nebulae to distinguish the characteristics of the red giant stellar winds that existed prior to their formation.

In this paper, we provide new, deep imaging of a number of multiple rings observed around WR stars in an optical narrow-band survey made of WR stars in the southern skies. We discuss their possible implications for WR evolution and postulate what further information they may provide about the evolution of massive stars with closer investigation.

2. OBSERVATIONS

Narrow-band imaging, using H α ($\lambda=6563 \text{ \AA}$, $\Delta\lambda=12 \text{ \AA}$) and [O III] ($\lambda=5006 \text{ \AA}$, $\Delta\lambda=44 \text{ \AA}$) filters was performed using a Thomson 1024 \times 1024 CCD chip at the f/3 focus of the 0.6 m Curtis Schmidt at Cerro Tololo Interamerican Observatory (CTIO) during the nights of 15–19 May 1994. The sample objects were taken from the lists of Marston et al. (1994) and Marston & Yocum (in preparation). It was intended that all possible shells associated with the WR stars would be identified as well as information on relative sizes and morphologies. A full listing of observations used in this paper are supplied in Table 1.

3. RESULTS ON MULTIPLE RINGS

Images of the multiple ring systems of our sample are shown in Figs. 1–5. These reveal nebulae whose morphologies allow a classification into two distinct types. Those with bipolar shapes in an outer ejecta shell, and those with more spherical outer shells. Table 2 lists the ring type (after Chu 1991) and apparent sizes of the multiple shells.

3.1 Bipolar Shells

Figures 1(a) and 1(b) show new, deep images of the nebula RCW 104 in both H α and [O III] which surrounds the WR star WR75. This is the only object in our sample to show a bipolar morphology in H α . However, close inspection of Fig. 1 of Marston et al. (1994) shows that the nebula NGC 2359 around the star WR6 has a diffuse outer, bipolar shell, which extends to approximately 20' from the central star. The bright shell in the center is only 5' across. NGC 2359 has been shown to have multiple velocity components which may be associated with multiple ejections (Goudfis et al. 1994). Ejected material appears to be interacting with the diffuse bipolar materials as well as a nearby molecular cloud (Marston 1991; Schneid et al. 1981). The shell around

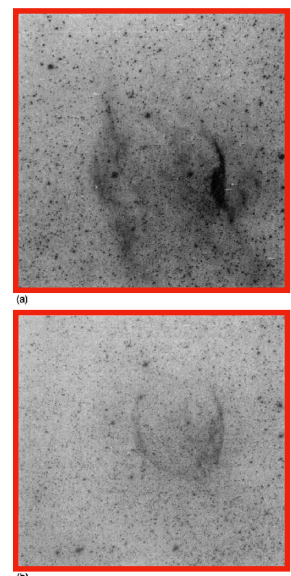


FIG. 1. (a) H α image of the filamentary, bipolar nebula RCW104 surrounding the WR star WR75. (b) Deep [O III] image of the wind-blown bubble at the center of RCW104.

“Digitization” = extraction of page objects such as:

- Tables
- Math formulas
- Figures
- Figure Captions

~ 50k initial page scans
~3 million potential articles
From ~1850-1997

NASA Astrophysics Data System

256

WOLFSON & VERMA

Vol. 375

tions in the x - y plane are vertical lines whose uneven spacing belies the presence of volume currents associated with the z -component of the field. For $\alpha > \pi$ the field topology changes, with cells containing field lines whose projections are closed loops (arcades) and islands. We will not be concerned further with these topologically distinct solutions, except to note that they do not arise until α exceeds π , with the $z=x$ straight-line solution separating them from the simple arcade solutions that shown in Figure 1.

The footpoint shear Δz for the constant- z solution is readily calculated. Equation (7) shows that the value of A on the field line whose footpoints are located at $\pm x_f$ is simply $\cos \pi x_f$. Then the equation for this field line can be written $\cos \pi x_f = \cos \pi x e^{-\sqrt{\pi^2 - x^2} y}$, so y as a function of x on the field line is given by

$$y_0(x) = \frac{\ln(\cos \pi x / \cos \pi x_f)}{\sqrt{\pi^2 - x^2}}, \quad (8)$$

where again the subscript 0 designates the constant- z solution. Using this result for y in the term $\partial A / \partial y$ that appears in equation (5) then gives a very simple result for the shear Δz expressed as a function of the footpoint coordinate x_f :

$$\Delta z(x_f) = \frac{2x}{\sqrt{\pi^2 - x^2}} x_f = \lambda x_f, \quad (9)$$

where we have defined λ by

$$\lambda \equiv \frac{2x}{\sqrt{\pi^2 - x^2}}. \quad (10)$$

Thus the shear is a simple linear function of footpoint location, a fact shown graphically in Priest (1982, Fig. 3.8) and again in our Figure 5.

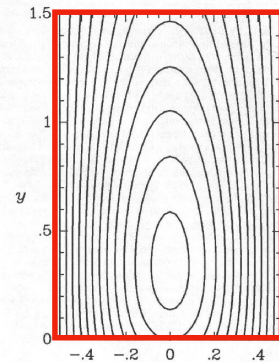


FIG. 3. Field lines projected into the x - y plane for the nonlinear solution $A = A_0 + \epsilon A_1$, with $\epsilon = 0.2$ and $\alpha = 3.0$. In this case the current enhancement is great enough to lead to magnetic islands, a situation that would be impossible in the time-averaged evolution of an ideal MHD system. Although the figure shows the oscillations what a closed-loop solution looks like, the assumptions leading to the perturbation expansion $A = A_0 + \epsilon A_1$ are violated before closed loops appear (see Fig. 4).

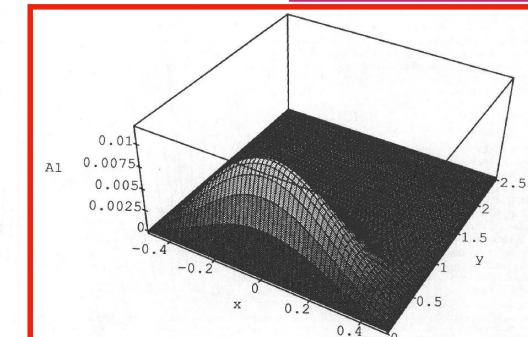


FIG. 2.—Plot of the perturbation solution $A_1(x, y)$, for $x = 0.5$. The single maximum corresponds to a region where current density is enhanced over the constant- z solution.

© American Astronomical Society • Provided by the NASA Astrophysics Data System

Version #2

What is the data?

WR star*	HD Number	Date observed	Filter	Exposure (secs)	Figure
WR16	HD86161	16 May 1994	H α	1800	2
WR30	HD94305	15 May 1994	H α	900	3a
WR30	-	19 May 1994	[O III]	2100	3b
WR40	HD96548	18 May 1994	H α	1800	4a
WR40	-	19 May 1994	[O III]	2100	4b
WR75	HD14749	17 May 1994	H α	2700	1a
WR75	-	17 May 1994	[O III]	2700	1b
WR85	HD8392B	16 May 1994	H α	900	5

* uses the nomenclature of van der Hucht et al. (1981).

ejection events. This uses a similar line of argument to that proposed by Balick *et al.* (1992) for using the extended halos of planetary nebulae to distinguish the characteristics of the red giant stellar winds that existed prior to their formation.

In this paper, we provide new, deep imaging of a number of multiple rings observed around WR stars in an optical narrow-band survey made of WR stars in the southern skies. We discuss their possible implications for WR evolution and postulate what further information they may provide about the evolution of massive stars with closer investigation.

2. OBSERVATIONS

Narrow-band imaging, using H α ($\lambda=6563\text{ \AA}$, $\Delta\lambda=12\text{ \AA}$) and [O III] ($\lambda=5006\text{ \AA}$, $\Delta\lambda=44\text{ \AA}$) filters was performed using a Thomson 1024 \times 1024 CCD chip at the $f/3$ focus of the 0.6 m Curtis Schmidt at Cerro Tololo Interamerican Observatory (CTIO) during the nights of 15–19 May 1994. The sample objects were taken from the lists of Marston *et al.* (1994) and Marston & Yocum (in preparation). It was intended that all possible shells associated with the WR stars would be identified as well as information on relative sizes and morphologies. A full listing of observations used in this paper are supplied in Table 1.

3. RESULTS ON MULTIPLE RINGS

Images of the multiple ring systems of our sample are shown in Figs. 1–5. These reveal nebulae whose morphologies allow a classification into two distinct types. Those with bipolar shapes in an outer ejecta shell, and those with more spherical outer shells. Table 2 lists the ring type (after Chu 1991) and apparent sizes of the multiple shells.

3.1 Bipolar Shells

Figures 1(a) and 1(b) show new, deep images of the nebula RCW 104 in both H α and [O III] which surrounds the WR star WR75. This is the only object in our sample to show a bipolar morphology in H α . However, close inspection of Fig. 1 of Marston *et al.* (1994) shows that the nebula NGC 2359 around the star WR6 has a diffuse outer, bipolar shell, which extends to approximately 20' from the central star. The bright shell in the center is only 5' across. NGC 2359 has been shown to have multiple velocity components which may be associated with multiple ejections (Gouliis *et al.* 1994). Ejected material appears to be interacting with the diffuse bipolar materials as well as a nearby molecular cloud (Marston 1991; Schneid *et al.* 1981). The shell around

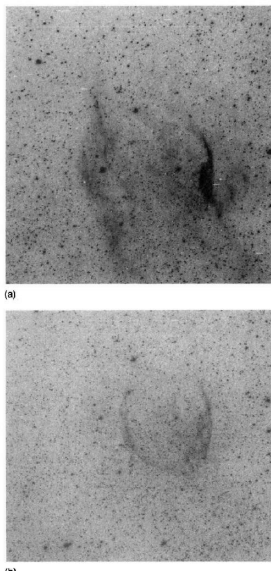


FIG. 1. (a) H α image of the filamentary, bipolar nebula RCW104 surrounding the WR star WR75. (b) Deep [O III] image of the wind-blown bubble at the center of RCW104.

WR75 shows similar multiple components. An outer bipolar flow is outlined by strong H α filaments in the central regions while fainter lobes are observed to the north and south, extending to around 15' from the central WN6 star. An inner ring of [O III] emitting material is observed entirely within the bipolar outflow and is only 10' in diameter. The outer filaments of RCW 104 have been spectroscopically observed by Esteban *et al.* (1990), who suggest their abundances are similar to that expected from the enhanced abundances in a RSG wind. We might interpret our observations of these two bipolar nebulae as being the RSG ejecta outer filaments and relatively young WR winds interacting with the ejecta to form central cavities. The expansion of the cavities has not yet reached the edge of the RSG ejecta.

In both cases of bipolar morphology, a wind-blown (W)

~ 50k initial page scans
~3 million potential articles
From ~1850-1997

NASA Astrophysics Data System

tions in the x - y plane are vertical lines whose uneven spacing belies the presence of volume currents associated with the z -component of the field. For $\alpha > \pi$ the field topology changes, with cells containing field lines whose projections are closed loops (arcades) and islands. We will not be concerned further with these topologically distinct solutions, except to note that they do not arise until α exceeds π , with the $z = \pi$ straight-line solution separating them from the simple arcade solutions like that shown in Figure 1.

The footpoint shear Δz for the constant- z solution is readily calculated. Equation (7) shows that the value of A on the field line whose footpoints are located at $\pm x_f$ is simply $\cos \pi x_f$. Then the equation for this field line can be written $\cos \pi x_f = \cos \pi x e^{-\sqrt{\pi^2 - x^2} y}$, so y as a function of x on the field line is given by

$$y_0(x) = \frac{\ln(\cos \pi x / \cos \pi x_f)}{\sqrt{\pi^2 - x^2}}, \quad (8)$$

where again the subscript 0 designates the constant- z solution. Using this result for y in the term $\partial A / \partial y$ that appears in equation (5) then gives a very simple result for the shear Δz expressed as a function of the footpoint coordinate x_f :

$$\Delta z(x_f) = \frac{2x}{\sqrt{\pi^2 - x^2}} x_f = \lambda x_f, \quad (9)$$

where we have defined λ by

$$\lambda \equiv \frac{2x}{\sqrt{\pi^2 - x^2}}. \quad (10)$$

Thus the shear is a simple linear function of footpoint location, a fact shown graphically in Priest (1982, Fig. 3.8) and again in our Figure 5.

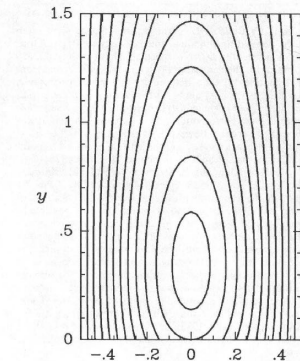


FIG. 3.—Field lines projected into the x - y plane for the nonlinear solution $A = A_0 + eA_1$, with $e = 0.2$ and $\alpha = 3.0$. In this case the current enhancement is great enough to lead to magnetic islands, a situation that would be impossible in the time-averaged electric field of an ideal MHD system. Although the figure is a simplification what a closed-loop perturbation looks like, the assumptions leading to the perturbation expansion $A = A_0 + eA_1$ are violated before closed loops appear (see Fig. 4).

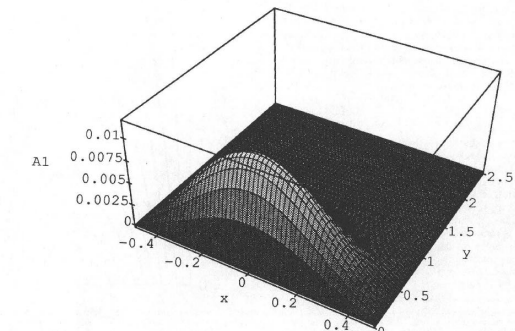


FIG. 2.—Plot of the perturbation solution $A_1(x, y)$ for $x = 0.5$. The single maximum corresponds to a region where current density is enhanced over the constant- z solution.

WR star*	HD Number	Date observed	Filter	Exposure (secs)	Figure
WR16	HD86161	16 May 1994	H α	1800	2
WR30	HD94305	15 May 1994	H α	900	3a
WR30	-	19 May 1994	[OIII]	2100	3b
WR40	HD96548	18 May 1994	H α	1800	4a
WR40	-	19 May 1994	[OIII]	2100	4b
WR75	HD14749	17 May 1994	H α	2700	1a
WR75	-	17 May 1994	[OIII]	2700	1b
WR85	HD8392B	16 May 1994	H α	900	5

* uses the nomenclature of van der Hucht et al. (1981).

ejection events. This uses a similar line of argument to that proposed by Balick et al. (1992) for using the extended halos of planetary nebulae to distinguish the characteristics of the red giant stellar winds that existed prior to their formation.

In this paper, we provide new, deep imaging of a number of multiple rings observed around WR stars in an optical narrow-band survey made of WR stars in the southern skies. We discuss their possible implications for WR evolution and postulate what further information they may provide about the evolution of massive stars with closer investigation.

2. OBSERVATIONS

Narrow-band imaging, using H α ($\lambda=6563\text{ \AA}$, $\Delta\lambda=12\text{ \AA}$) and [O III] ($\lambda=5006\text{ \AA}$, $\Delta\lambda=44\text{ \AA}$) filters was performed using a Thomson 1024 \times 1024 CCD chip at the $f/3$ focus of the 0.6 m Curtis Schmidt at Cerro Tololo Interamerican Observatory (CTIO) during the nights of 15–19 May 1994. The sample objects were taken from the lists of Marston et al. (1994) and Marston & Yocum (in preparation). It was intended that all possible shells associated with the WR stars would be identified as well as information on relative sizes and morphologies. A full listing of observations used in this paper are supplied in Table 1.

3. RESULTS ON MULTIPLE RINGS

Images of the multiple ring systems of our sample are shown in Figs. 1–5. These reveal nebulae whose morphologies allow a classification into two distinct types. Those with bipolar shapes in an outer ejecta shell, and those with more spherical outer shells. Table 2 lists the ring type (after Chu 1991) and apparent sizes of the multiple shells.

3.1 Bipolar Shells

Figures 1(a) and 1(b) show new, deep images of the nebula RCW 104 in both H α and [O III] which surrounds the WR star WR75. This is the only object in our sample to show a bipolar morphology in H α . However, close inspection of Fig. 1 of Marston et al. (1994) shows that the nebula NGC 2359 around the star WR6 has a diffuse outer, bipolar shell, which extends to approximately 20' from the central star. The bright shell in the center is only 5' across. NGC 2359 has been shown to have multiple velocity components which may be associated with multiple ejections (Gouliis et al. 1994). Ejected material appears to be interacting with the diffuse bipolar materials as well as a nearby molecular cloud (Marston 1991; Schneid et al. 1981). The shell around

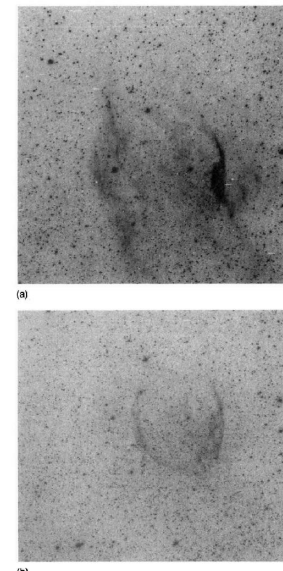


FIG. 1.—(a) H α image of the filamentary, bipolar nebula RCW104 surrounding the WR star WR75. (b) Deep [O III] image of the wind-blown bubble at the center of RCW104.

WR75 shows similar multiple components. An outer bipolar flow is outlined by strong H α filaments in the central regions while fainter lobes are observed to the north and south, extending to around 15' from the central WN6 star. An inner ring of [O III] emitting material is observed entirely within the bipolar outflow and is only 10' in diameter. The outer filaments of RCW 104 have been spectroscopically observed by Esteban et al. (1990), who suggest their abundances are similar to that expected from the enhanced abundances in a RSG wind. We might interpret our observations of these two bipolar nebulae as being the RSG ejecta outer filaments and relatively young WR winds interacting with the ejecta to form central cavities. The expansion of the cavities has not yet reached the edge of the RSG ejecta.

In both cases of bipolar morphology, a wind-blown (W)

What is the data?

“Digitization” = extraction
of page objects such as:

1840

256

WOLFSON & VERMA

Vol. 375

tions in the x - y plane are vertical lines whose uneven spacing belies the presence of volume currents associated with the z -component of the field. For $\alpha > \pi$ the field topology changes, with cells containing field lines whose projections are closed loops (arcades) and islands. We will not be concerned further with these topologically distinct solutions, except to note that they do not arise until α exceeds π , with the $z=x$ straight-line solution separating them from the simple arcade solutions that shown in Figure 1.

The footpoint shear Δz for the constant- z solution is readily calculated. Equation (7) shows that the value of A on the field line whose footpoints are located at $\pm x_f$ is simply $\cos \pi x_f$. Then the equation for this field line can be written $\cos \pi x_f = \cos \pi x e^{-\sqrt{x^2 - z^2} x_f}$, so y as a function of x on the field line is given by

$$y_0(x) = \frac{\ln(\cos \pi x / \cos \pi x_f)}{\sqrt{\pi^2 - x^2}}, \quad (8)$$

where again the subscript 0 designates the constant- z solution. Using this result for y in the term $\partial A / \partial y$ that appears in equation (5) then gives a very simple result for the shear Δz expressed as a function of the footpoint coordinate x_f :

$$\Delta z(x_f) = \frac{2x}{\sqrt{\pi^2 - x^2}} x_f = \lambda x_f, \quad (9)$$

where we have defined λ by

$$\lambda \equiv \frac{2x}{\sqrt{\pi^2 - x^2}}. \quad (10)$$

Thus the shear is a simple linear function of footpoint location, a fact shown graphically in Priest (1982, Fig. 3.8) and again in our Figure 5.

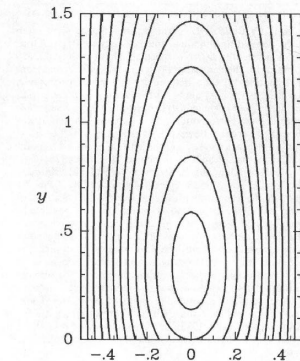


FIG. 3.—Field lines projected into the x - y plane for the nonlinear solution $A = A_0 + eA_1$, with $e = 0.2$ and $\alpha = 3.0$. In this case the current enhancement is great enough to lead to magnetic islands, a situation that would be impossible in the time-averaged evolution of an ideal MHD system. Although the figure is a simplification what a closed-loop perturbation looks like, the assumptions leading to the perturbation expansion $A = A_0 + eA_1$ are violated before closed loops appear (see Fig. 4).

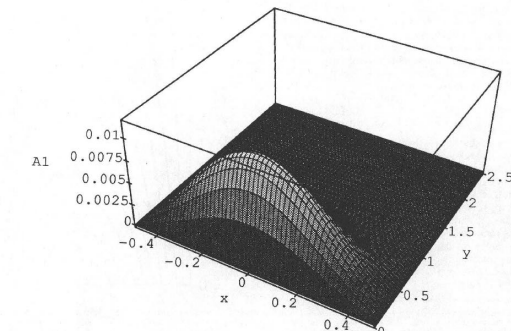


FIG. 2.—Plot of the perturbation solution $A_1(x, y)$ for $x = 0.5$. The single maximum corresponds to a region where current density is enhanced over the constant- z solution.

© American Astronomical Society • Provided by the NASA Astrophysics Data System

NASA Astrophysics Data System

© American Astronomical Society • Provided by the NASA Astrophysics Data System

What is the data?

1840 A. R. MARSTON: RINGS AROUND WR STARS

WR star*	HD Number	Date observed	Filter	Exposure (secs)	Figure
WR16	HD86161	16 May 1994	H α	1800	2
WR30	HD94305	15 May 1994	H α	900	3a
WR30	-	19 May 1994	[OIII]	2100	3b
WR40	HD96548	18 May 1994	H α	1800	4a
WR40	-	19 May 1994	[OIII]	2100	4b
WR75	HD14749	17 May 1994	H α	2700	1a
WR75	-	17 May 1994	[OIII]	2700	1b
WR85	HD8392B	16 May 1994	H α	900	5

* uses the nomenclature of van der Hucht et al. (1981).

ejection events. This uses a similar line of argument to that proposed by Balick et al. (1992) for using the extended halos of planetary nebulae to distinguish the characteristics of the red giant stellar winds that existed prior to their formation.

In this paper, we provide new, deep imaging of a number of multiple rings observed around WR stars in an optical narrow-band survey made of WR stars in the southern skies. We discuss their possible implications for WR evolution and postulate what further information they may provide about the evolution of massive stars with closer investigation.

2. OBSERVATIONS

Narrow-band imaging, using H α ($\lambda=6563 \text{ \AA}$, $\Delta\lambda=12 \text{ \AA}$) and [O III] ($\lambda=5006 \text{ \AA}$, $\Delta\lambda=44 \text{ \AA}$) filters was performed using a Thomson 1024 \times 1024 CCD chip at the $f/3$ focus of the 0.6 m Curtis Schmidt at Cerro Tololo Interamerican Observatory (CTIO) during the nights of 15–19 May 1994. The sample objects were taken from the lists of Marston et al. (1994) and Marston & Yocum (in preparation). It was intended that all possible shells associated with the WR stars would be identified as well as information on relative sizes and morphologies. A full listing of observations used in this paper are supplied in Table 1.

3. RESULTS ON MULTIPLE RINGS

Images of the multiple ring systems of our sample are shown in Figs. 1–5. These reveal nebulae whose morphologies allow a classification into two distinct types. Those with bipolar shapes in an outer ejecta shell, and those with more spherical outer shells. Table 2 lists the ring type (after Chu 1991) and apparent sizes of the multiple shells.

3.1 Bipolar Shells

Figures 1(a) and 1(b) show new, deep images of the nebula RCW 104 in both H α and [O III] which surrounds the WR star WR75. This is the only object in our sample to show a bipolar morphology in H α . However, close inspection of Fig. 1 of Marston et al. (1994) shows that the nebula NGC 2359 around the star WR6 has a diffuse outer, bipolar shell, which extends to approximately 20' from the central star. The bright shell in the center is only 5' across. NGC 2359 has been shown to have multiple velocity components which may be associated with multiple ejections (Gouliis et al. 1994). Ejected material appears to be interacting with the diffuse bipolar materials as well as a nearby molecular cloud (Marston 1991; Schneid et al. 1981). The shell around

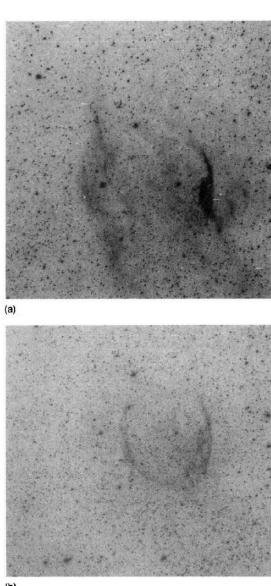


FIG. 1.—(a) H α image of the filamentary, bipolar nebula RCW104 surrounding the WR star WR75. (b) Deep [O III] image of the wind-blown bubble at the center of RCW104.

WR75 shows similar multiple components. An outer bipolar flow is outlined by strong H α filaments in the central regions while fainter lobes are observed to the north and south, extending to around 15' from the central WN6 star. An inner ring of [O III] emitting material is observed entirely within the bipolar outflow and is only 10' in diameter. The outer filaments of RCW 104 have been spectroscopically observed by Esteban et al. (1990), who suggest their abundances are similar to that expected from the enhanced abundances in a RSG wind. We might interpret our observations of these two bipolar nebulae as being the RSG ejecta outer filaments and relatively young WR winds interacting with the ejecta to form central cavities. The expansion of the cavities has not yet reached the edge of the RSG ejecta.

In both cases of bipolar morphology, a wind-blown (W)

“Digitization” = extraction
of page objects such as:

- Tables

~ 50k initial page scans
~3 million potential articles
From ~1850-1997

256

WOLFSON & VERMA

Vol. 375

tions in the x - y plane are vertical lines whose uneven spacing belies the presence of volume currents associated with the z -component of the field. For $\alpha > \pi$ the field topology changes, with cells containing field lines whose projections are closed loops (arcades) and islands. We will not be concerned further with these topologically distinct solutions, except to note that they do not arise until α exceeds π , with the $z = \pi$ straight-line solution separating them from the simple arcade solutions that shown in Figure 1.

The footpoint shear Δz for the constant- z solution is readily calculated. Equation (7) shows that the value of A on the field line whose footpoints are located at $\pm x_f$ is simply $\cos \pi x_f$. Then the equation for this field line can be written $\cos \pi x_f = \cos \pi x e^{-\sqrt{\pi^2 - x^2} x_f}$, so y as a function of x on the field line is given by

$$y_0(x) = \frac{\ln(\cos \pi x / \cos \pi x_f)}{\sqrt{\pi^2 - x^2}}, \quad (8)$$

where again the subscript 0 designates the constant- z solution. Using this result for y in the term $\partial A / \partial y$ that appears in equation (5) then gives a very simple result for the shear Δz expressed as a function of the footpoint coordinate x_f :

$$\Delta z(x_f) = \frac{2x}{\sqrt{\pi^2 - x^2}} x_f = \lambda x_f, \quad (9)$$

where we have defined λ by

$$\lambda \equiv \frac{2x}{\sqrt{\pi^2 - x^2}}. \quad (10)$$

Thus the shear is a simple linear function of footpoint location, a fact shown graphically in Priest (1982, Fig. 3.8) and again in our Figure 5.

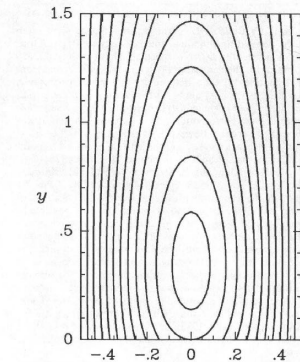


FIG. 3.—Field lines projected into the x - y plane for the nonlinear solution $A = A_0 + eA_1$, with $e = 0.2$ and $\alpha = 3.0$. In this case the current enhancement is great enough to lead to magnetic islands, a situation that would be impossible in the time-averaged energy of an ideal MHD system. Although the figure is a simplification what a closed-loop perturbation looks like, the assumptions leading to the perturbation expansion $A = A_0 + eA_1$ are violated before closed loops appear (see Fig. 4).

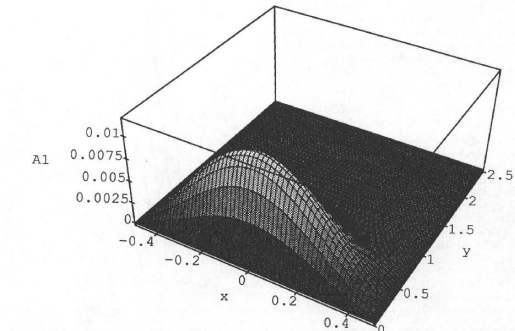


FIG. 2.—Plot of the perturbation solution $A_1(x, y)$, for $x = 0.5$. The single maximum corresponds to a region where current density is enhanced over the constant- z solution.

© American Astronomical Society • Provided by the NASA Astrophysics Data System

NASA Astrophysics Data System

What is the data?

1840 A. R. MARSTON: RINGS AROUND WR STARS

WR star*	HD Number	Date observed	Filter	Exposure (secs)	Figure
WR16	HD86161	16 May 1994	H α	1800	2
WR30	HD94305	15 May 1994	H α	900	3a
WR30	-	19 May 1994	[OIII]	2100	3b
WR40	HD96548	18 May 1994	H α	1800	4a
WR40	-	19 May 1994	[OIII]	2100	4b
WR75	HD14749	17 May 1994	H α	2700	1a
WR75	-	17 May 1994	[OIII]	2700	1b
WR85	HD8392B	16 May 1994	H α	900	5

* uses the nomenclature of van der Hucht et al. (1981).

ejection events. This uses a similar line of argument to that proposed by Balick et al. (1992) for using the extended halos of planetary nebulae to distinguish the characteristics of the red giant stellar winds that existed prior to their formation.

In this paper, we provide new, deep imaging of a number of multiple rings observed around WR stars in an optical narrow-band survey made of WR stars in the southern skies. We discuss their possible implications for WR evolution and postulate what further information they may provide about the evolution of massive stars with closer investigation.

2. OBSERVATIONS

Narrow-band imaging, using H α ($\lambda=6563$ Å, $\Delta\lambda=12$ Å) and [O III] ($\lambda=5006$ Å, $\Delta\lambda=44$ Å) filters was performed using a Thomson 1024×1024 CCD chip at the $f/3$ focus of the 0.6 m Curtis Schmidt at Cerro Tololo Interamerican Observatory (CTIO) during the nights of 15–19 May 1994. The sample objects were taken from the lists of Marston et al. (1994) and Marston & Yocum (in preparation). It was intended that all possible shells associated with the WR stars would be identified as well as information on relative sizes and morphologies. A full listing of observations used in this paper are supplied in Table 1.

3. RESULTS ON MULTIPLE RINGS

Images of the multiple ring systems of our sample are shown in Figs. 1–5. These reveal nebulae whose morphologies allow a classification into two distinct types. Those with bipolar shapes in an outer ejecta shell, and those with more spherical outer shells. Table 2 lists the ring type (after Chu 1991) and apparent sizes of the multiple shells.

3.1 Bipolar Shells

Figures 1(a) and 1(b) show new, deep images of the nebula RCW 104 in both H α and [O III] which surrounds the WR star WR75. This is the only object in our sample to show a bipolar morphology in H α . However, close inspection of Fig. 1 of Marston et al. (1994) shows that the nebula NGC 2359 around the star WR6 has a diffuse outer, bipolar shell, which extends to approximately 20' from the central star. The bright shell in the center is only 5' across. NGC 2359 has been shown to have multiple velocity components which may be associated with multiple ejections (Gouliis et al. 1994). Ejected material appears to be interacting with the diffuse bipolar materials as well as a nearby molecular cloud (Marston 1991; Schneid et al. 1981). The shell around

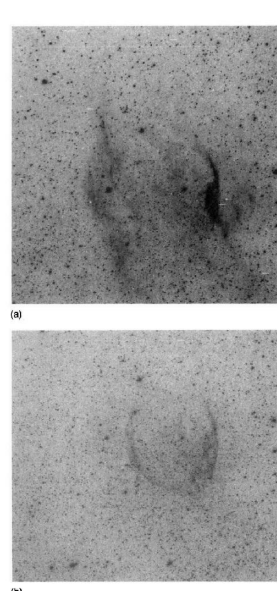


FIG. 1.—(a) H α image of the filamentary, bipolar nebula RCW104 surrounding the WR star WR75. (b) Deep [O III] image of the wind-blown bubble at the center of RCW104.

WR75 shows similar multiple components. An outer bipolar flow is outlined by strong H α filaments in the central regions while fainter lobes are observed to the north and south, extending to around 15' from the central WN6 star. An inner ring of [O III] emitting material is observed entirely within the bipolar outflow and is only 10' in diameter. The outer filaments of RCW 104 have been spectroscopically observed by Esteban et al. (1990), who suggest their abundances are similar to that expected from the enhanced abundances in a RSG wind. We might interpret our observations of these two bipolar nebulae as being the RSG ejecta outer filaments and relatively young WR winds interacting with the ejecta to form central cavities. The expansion of the cavities has not yet reached the edge of the RSG ejecta.

In both cases of bipolar morphology, a wind-blown (W)

“Digitization” = extraction
of page objects such as:

- Tables
- Math formulas

~ 50k initial page scans
~3 million potential articles
From ~1850-1997

NASA Astrophysics Data System

256

WOLFSON & VERMA

Vol. 375

tions in the x - y plane are vertical lines whose uneven spacing belies the presence of volume currents associated with the z -component of the field. For $\alpha > \pi$ the field topology changes, with cells containing field lines whose projections are closed loops (arcades) and islands. We will not be concerned further with these topologically distinct solutions, except to note that they do not arise until α exceeds π , with the $z = \pi$ straight-line solution separating them from the simple arcade solutions that shown in Figure 1.

The footpoint shear Δz for the constant- z solution is readily calculated. Equation (7) shows that the value of A on the field line whose footpoints are located at $\pm x_f$ is simply $\cos \pi x_f$. Then the equation for this field line can be written $\cos \pi x_f = \cos \pi x e^{-\sqrt{\pi^2 - x^2} y}$, so y as a function of x on the field line is given by

$$y_0(x) = \frac{\ln(\cos \pi x / \cos \pi x_f)}{\sqrt{\pi^2 - x^2}}, \quad (8)$$

where again the subscript 0 designates the constant- z solution. Using this result for y in the term $\partial A / \partial y$ that appears in equation (5) then gives a very simple result for the shear Δz expressed as a function of the footpoint coordinate x_f :

$$\Delta z(x_f) = \frac{2x}{\sqrt{\pi^2 - x^2}} x_f = \lambda x_f, \quad (9)$$

where we have defined λ by

$$\lambda \equiv \frac{2x}{\sqrt{\pi^2 - x^2}}. \quad (10)$$

Thus the shear is a simple linear function of footpoint location, a fact shown graphically in Priest (1982, Fig. 3.8) and again in our Figure 5.

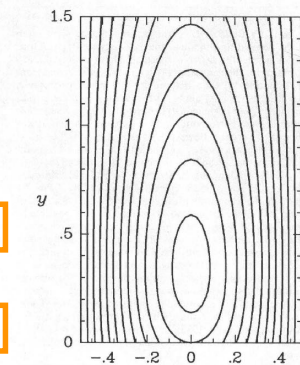


FIG. 3.—Field lines projected into the x - y plane for the nonlinear solution $A = A_0 + eA_1$, with $e = 0.2$ and $\alpha = 3.0$. In this case the current enhancement is great enough to lead to magnetic islands, a situation that would be impossible in the time-averaged electric field of an ideal MHD system. Although the figure does not illustrate what a closed-loop perturbation looks like, the assumptions leading to the perturbation expansion $A = A_0 + eA_1$ are violated before closed loops appear (see Fig. 4).

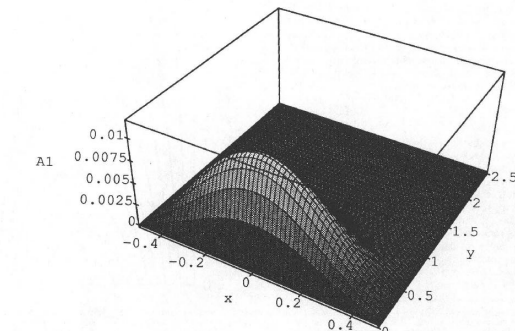


FIG. 2.—Plot of the perturbation solution $A_1(x, y)$, for $x = 0.5$. The single maximum corresponds to a region where current density is enhanced over the constant- z solution.

© American Astronomical Society • Provided by the NASA Astrophysics Data System

What is the data?

1840 A. R. MARSTON: RINGS AROUND WR STARS

WR star*	HD Number	Date observed	Filter	Exposure (secs)	Figure
WR16	HD86161	16 May 1994	H α	1800	2
WR30	HD94305	15 May 1994	H α	900	3a
WR30	-	19 May 1994	[O III]	2100	3b
WR40	HD96548	18 May 1994	H α	1800	4a
WR40	-	19 May 1994	[O III]	2100	4b
WR75	HD14749	17 May 1994	H α	2700	1a
WR75	-	17 May 1994	[O III]	2700	1b
WR85	HD8392B	16 May 1994	H α	900	5

* uses the nomenclature of van der Hucht et al. (1981).

ejection events. This uses a similar line of argument to that proposed by Balick *et al.* (1992) for using the extended halos of planetary nebulae to distinguish the characteristics of the red giant stellar winds that existed prior to their formation.

In this paper, we provide new, deep imaging of a number of multiple rings observed around WR stars in an optical narrow-band survey made of WR stars in the southern skies. We discuss their possible implications for WR evolution and postulate what further information they may provide about the evolution of massive stars with closer investigation.

2. OBSERVATIONS

Narrow-band imaging, using H α ($\lambda=6563\text{ \AA}$, $\Delta\lambda=12\text{ \AA}$) and [O III] ($\lambda=5006\text{ \AA}$, $\Delta\lambda=44\text{ \AA}$) filters was performed using a Thomson 1024 \times 1024 CCD chip at the $f/3$ focus of the 0.6 m Curtis Schmidt at Cerro Tololo Interamerican Observatory (CTIO) during the nights of 15–19 May 1994. The sample objects were taken from the lists of Marston *et al.* (1994) and Marston & Yocum (in preparation). It was intended that all possible shells associated with the WR stars would be identified as well as information on relative sizes and morphologies. A full listing of observations used in this paper are supplied in Table 1.

3. RESULTS ON MULTIPLE RINGS

Images of the multiple ring systems of our sample are shown in Figs. 1(a)–1(b). These reveal nebulae whose morphologies allow a classification into two distinct types. Those with bipolar shapes in an outer ejecta shell, and those with more spherical outer shells. Table 2 lists the ring type (after Chu 1991) and apparent sizes of the multiple shells.

3.1 Bipolar Shells

Figures 1(a) and 1(b) show new, deep images of the nebula RCW 104 in both H α and [O III] which surrounds the WR star WR75. This is the only object in our sample to show a bipolar morphology in H α . However, close inspection of Fig. 1 of Marston *et al.* (1994) shows that the nebula NGC 2359 around the star WR6 has a diffuse outer, bipolar shell, which extends to approximately 20' from the central star. The bright shell in the center is only 5' across. NGC 2359 has been shown to have multiple velocity components which may be associated with multiple ejections (Goulielmos *et al.* 1994). Ejected material appears to be interacting with the diffuse bipolar materials as well as a nearby molecular cloud (Marston 1991; Schneid *et al.* 1981). The shell around

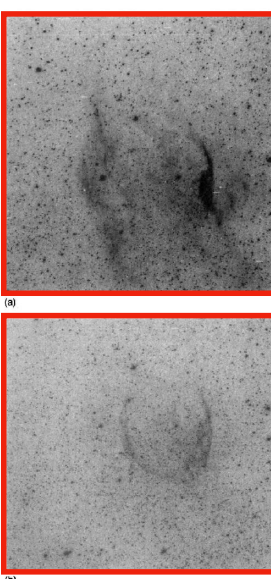


FIG. 1. (a) H α image of the filamentary, bipolar nebula RCW104 surrounding the WR star WR75. (b) Deep [O III] image of the wind-blown bubble at the center of RCW104.

“Digitization” = extraction of page objects such as:

- Tables
- Math formulas
- Figures

256

WOLFSON & VERMA

Vol. 375

tions in the x - y plane are vertical lines whose uneven spacing belies the presence of volume currents associated with the z -component of the field. For $\alpha > \pi$ the field topology changes, with cells containing field lines whose projections are closed loops (arcades) and islands. We will not be concerned further with these topologically distinct solutions, except to note that they do not arise until α exceeds π , with the $z=x$ straight-line solution separating them from the simple arcade solutions that shown in Figure 1.

The footpoint shear Δz for the constant- z solution is readily calculated. Equation (7) shows that the value of A on the field line whose footpoints are located at $\pm x_f$ is simply $\cos \pi x_f$. Then the equation for this field line can be written $\cos \pi x_f = \cos \pi x e^{-\sqrt{\pi^2 - x^2} x}$, so y as a function of x on the field line is given by

$$y_0(x) = \frac{\ln(\cos \pi x / \cos \pi x_f)}{\sqrt{\pi^2 - x^2}}, \quad (8)$$

where again the subscript 0 designates the constant- z solution. Using this result for y in the term $\partial A / \partial y$ that appears in equation (5) then gives a very simple result for the shear Δz expressed as a function of the footpoint coordinate x_f :

$$\Delta z(x_f) = \frac{2x}{\sqrt{\pi^2 - x^2}} x_f = \lambda x_f, \quad (9)$$

where we have defined λ by

$$\lambda \equiv \frac{2x}{\sqrt{\pi^2 - x^2}}. \quad (10)$$

Thus the shear is a simple linear function of footpoint location, a fact shown graphically in Priest (1982, Fig. 3.8) and again in our Figure 5.

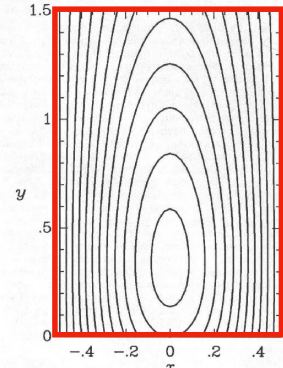


FIG. 3.—Field lines projected into the x - y plane for the nonlinear solution $A = A_0 + eA_1$, with $e = 0.2$ and $\alpha = 3.0$. In this case the current enhancement is great enough to lead to magnetic islands, a situation that would be impossible in the time-averaged energy of an ideal MHD system. Although the figure does not illustrate what a closed-loop perturbation looks like, the assumptions leading to the perturbation expansion $A = A_0 + eA_1$ are violated before closed loops appear (see Fig. 4).

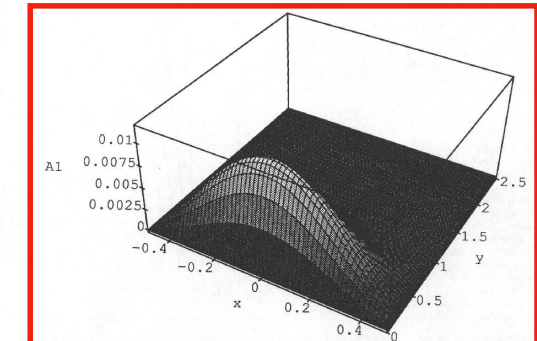


FIG. 4.—Plot of the perturbation solution $A_1(x, y)$, for $x = 0.5$. The single maximum corresponds to a region where current density is enhanced over the constant- z solution.

© American Astronomical Society • Provided by the NASA Astrophysics Data System

~ 50k initial page scans
~3 million potential articles
From ~1850-1997

NASA Astrophysics Data System

© American Astronomical Society • Provided by the NASA Astrophysics Data System

What is the data?

1840 A. R. MARSTON: RINGS AROUND WR STARS

WR star*	HD Number	Date observed	Filter	Exposure (secs)	Figure
WR16	HD86161	16 May 1994	H α	1800	2
WR30	HD94305	15 May 1994	H α	900	3a
WR30	-	19 May 1994	[O III]	2100	3b
WR40	HD96548	18 May 1994	H α	1800	4a
WR40	-	19 May 1994	[O III]	2100	4b
WR75	HD14749	17 May 1994	H α	2700	1a
WR75	-	17 May 1994	[O III]	2700	1b
WR85	HD8392B	16 May 1994	H α	900	5

* uses the nomenclature of van der Hucht et al. (1981).

ejection events. This uses a similar line of argument to that proposed by Balick et al. (1992) for using the extended halos of planetary nebulae to distinguish the characteristics of the red giant stellar winds that existed prior to their formation.

In this paper, we provide new, deep imaging of a number of multiple rings observed around WR stars in an optical narrow-band survey made of WR stars in the southern skies. We discuss their possible implications for WR evolution and postulate what further information they may provide about the evolution of massive stars with closer investigation.

2. OBSERVATIONS

Narrow-band imaging, using H α ($\lambda=6563 \text{ \AA}$, $\Delta\lambda=12 \text{ \AA}$) and [O III] ($\lambda=5006 \text{ \AA}$, $\Delta\lambda=44 \text{ \AA}$) filters was performed using a Thomson 1024 \times 1024 CCD chip at the f/3 focus of the 0.6 m Curtis Schmidt at Cerro Tololo Interamerican Observatory (CTIO) during the nights of 15–19 May 1994. The sample objects were taken from the lists of Marston et al. (1994) and Marston & Yocum (in preparation). It was intended that all possible shells associated with the WR stars would be identified as well as information on relative sizes and morphologies. A full listing of observations used in this paper are supplied in Table 1.

3. RESULTS ON MULTIPLE RINGS

Images of the multiple ring systems of our sample are shown in Figs. 1–5. These reveal nebulae whose morphologies allow a classification into two distinct types. Those with bipolar shapes in an outer ejecta shell, and those with more spherical outer shells. Table 2 lists the ring type (after Chu 1991) and apparent sizes of the multiple shells.

3.1 Bipolar Shells

Figures 1(a) and 1(b) show new, deep images of the nebula RCW 104 in both H α and [O III] which surrounds the WR star WR75. This is the only object in our sample to show a bipolar morphology in H α . However, close inspection of Fig. 1 of Marston et al. (1994) shows that the nebula NGC 2359 around the star WR6 has a diffuse outer, bipolar shell, which extends to approximately 20' from the central star. The bright shell in the center is only 5' across. NGC 2359 has been shown to have multiple velocity components which may be associated with multiple ejections (Goudfis et al. 1994). Ejected material appears to be interacting with the diffuse bipolar materials as well as a nearby molecular cloud (Marston 1991; Schneid et al. 1981). The shell around

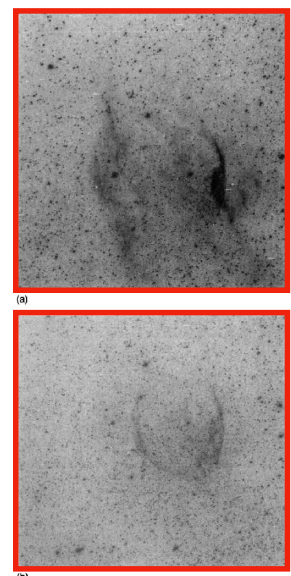


FIG. 1. (a) H α image of the filamentary, bipolar nebula RCW104 surrounding the WR star WR75. (b) Deep [O III] image of the wind-blown bubble at the center of RCW104.

“Digitization” = extraction of page objects such as:

- Tables
- Math formulas
- Figures
- Figure Captions

~ 50k initial page scans
~3 million potential articles
From ~1850-1997

NASA Astrophysics Data System

256

WOLFSON & VERMA

Vol. 375

tions in the x - y plane are vertical lines whose uneven spacing belies the presence of volume currents associated with the z -component of the field. For $\alpha > \pi$ the field topology changes, with cells containing field lines whose projections are closed loops (arcades) and islands. We will not be concerned further with these topologically distinct solutions, except to note that they do not arise until α exceeds π , with the $z=x$ straight-line solution separating them from the simple arcade solutions that shown in Figure 1.

The footpoint shear Δz for the constant- z solution is readily calculated. Equation (7) shows that the value of A on the field line whose footpoints are located at $\pm x_f$ is simply $\cos \pi x_f$. Then the equation for this field line can be written $\cos \pi x_f = \cos \pi x e^{-\sqrt{\pi^2 - x^2} y}$, so y as a function of x on the field line is given by

$$y_0(x) = \frac{\ln(\cos \pi x / \cos \pi x_f)}{\sqrt{\pi^2 - x^2}}, \quad (8)$$

where again the subscript 0 designates the constant- z solution. Using this result for y in the term $\partial A / \partial y$ that appears in equation (5) then gives a very simple result for the shear Δz expressed as a function of the footpoint coordinate x_f :

$$\Delta z(x_f) = \frac{2x}{\sqrt{\pi^2 - x^2}} x_f = \lambda x_f, \quad (9)$$

where we have defined λ by

$$\lambda \equiv \frac{2x}{\sqrt{\pi^2 - x^2}}. \quad (10)$$

Thus the shear is a simple linear function of footpoint location, a fact shown graphically in Priest (1982, Fig. 3.8) and again in our Figure 5.

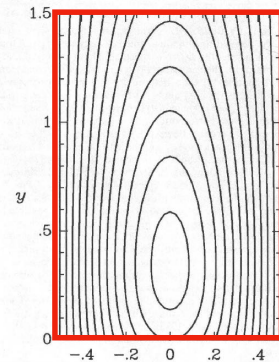


FIG. 3. Field lines projected into the x - y plane for the nonlinear solution $A = A_0 + \epsilon A_1$, with $\epsilon = 0.2$ and $\alpha = 3.0$. In this case the current enhancement is great enough to lead to magnetic islands, a situation that would be impossible in the time-averaged evolution of an ideal MHD system. Although the figure shows the oscillations what a closed-loop solution looks like, the assumptions leading to the perturbation expansion $A = A_0 + \epsilon A_1$ are violated before closed loops appear (see Fig. 4).

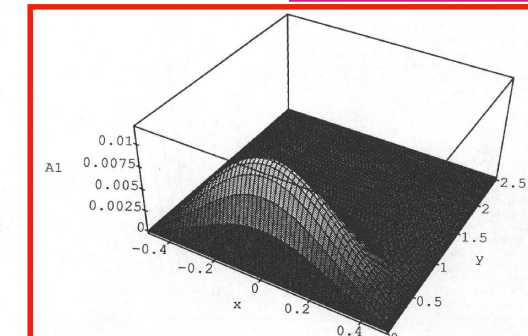


FIG. 2.—Plot of the perturbation solution $A_1(x, y)$, for $x = 0.5$. The single maximum corresponds to a region where current density is enhanced over the constant- z solution.

© American Astronomical Society • Provided by the NASA Astrophysics Data System

What did we notice about the differences between Version #1 and Version #2?

Example 2: Audience Engagement with Foundational Concepts

Version #1

Object Detection for Figures in Articles



Object Detection for Figures in Articles

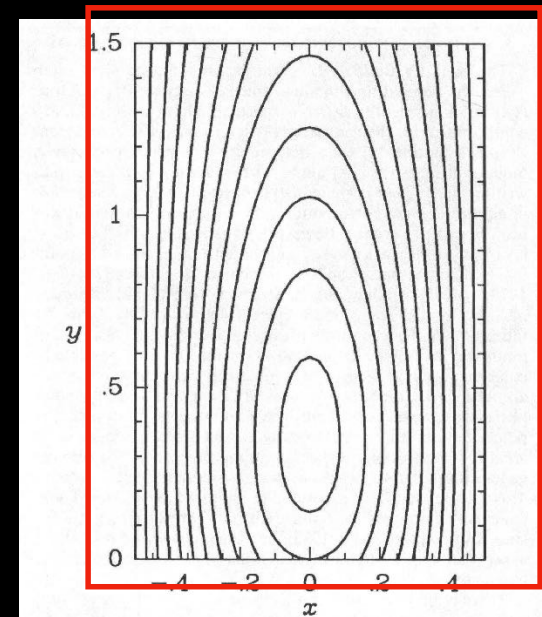


FIG. 3.—Field lines projected into the x - y plane for the nonlinear solution $A = A_0 + \epsilon A_1$, with $\epsilon = 0.2$ and $\alpha = 3.02$. In this case the current enhancement is great enough to lead to magnetic islands, a situation that would be impossible in the temporal evolution of an ideal MHD system. Although the figure illustrates qualitatively what a closed-loop solution looks like, the assumptions leading to the perturbation expansion $A = A_0 + \epsilon A_1$ are violated before closed loops appear (see Fig. 4).

Version #2

Object detection “works” differently with figures in journal articles.

Let's play a game...

Let's play a game...

Is this a dog?

Let's play a game...

Is this a dog?

HAND



Raise your hand if you see a dog:

NO HAND



DO NOT raise your hand if the image is not a dog:

Let's play a game...

Is this a dog? Raise your hand if you see a dog:

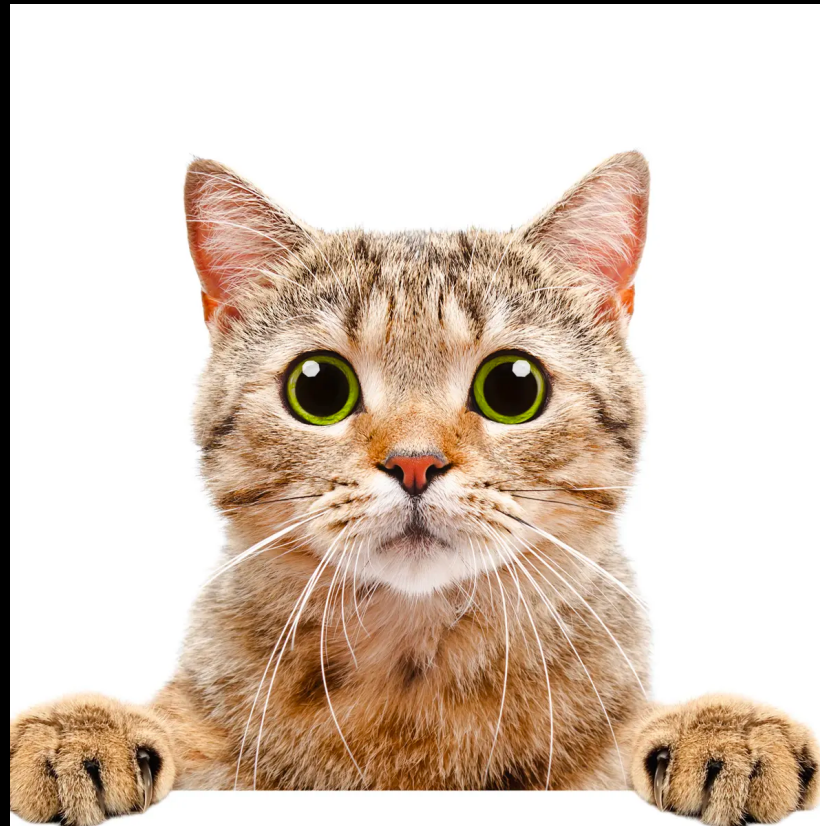
Let's play a game...

Is this a dog? Raise your hand if you see a dog:



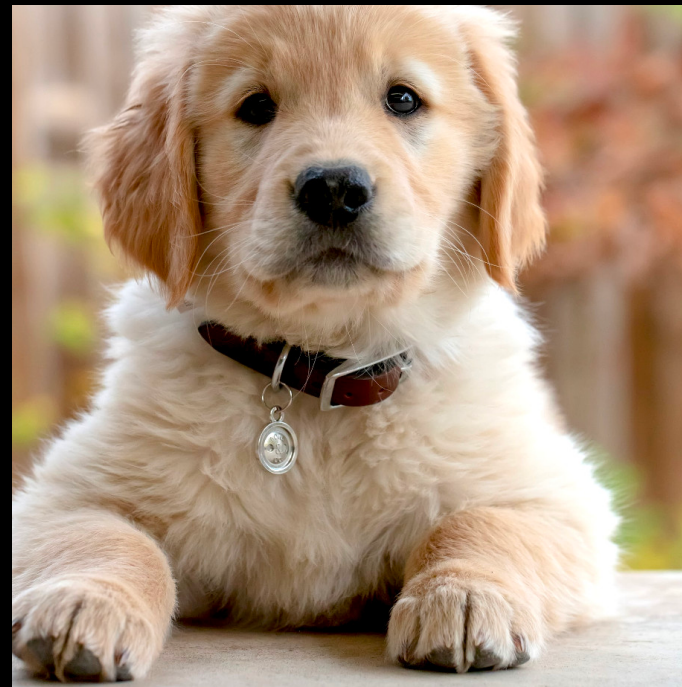
Let's play a game...

Is this a dog? Raise your hand if you see a dog:



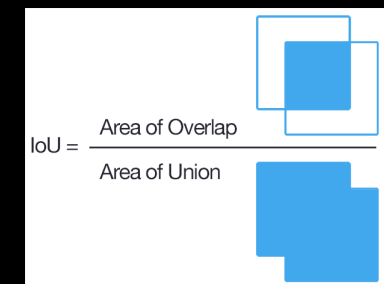
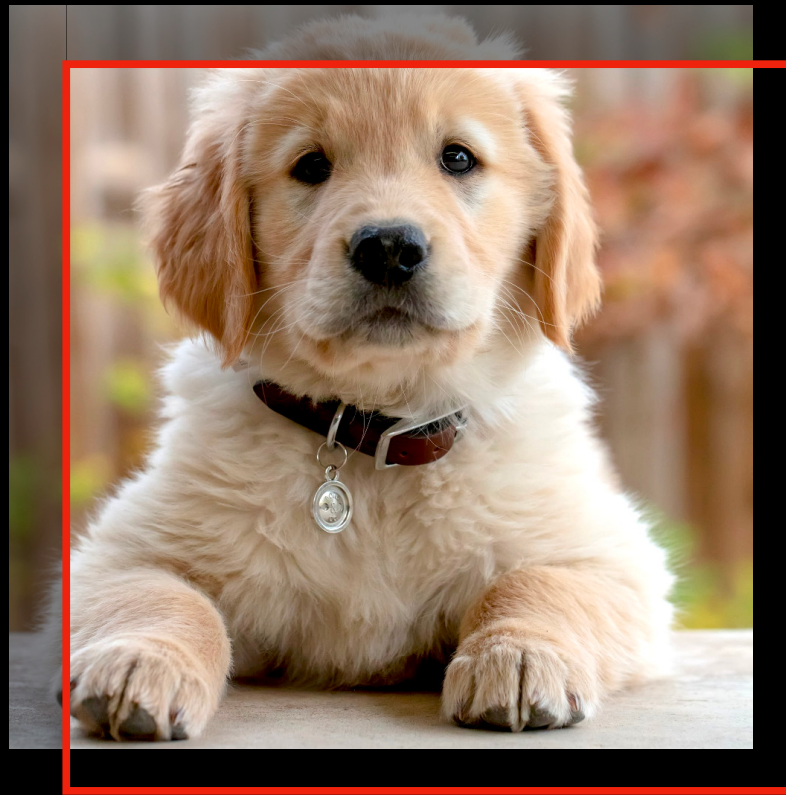
Let's play a game...

Is this a dog? Raise your hand if you see a dog:



Let's play a game...

Is this a dog? Raise your hand if you see a dog:

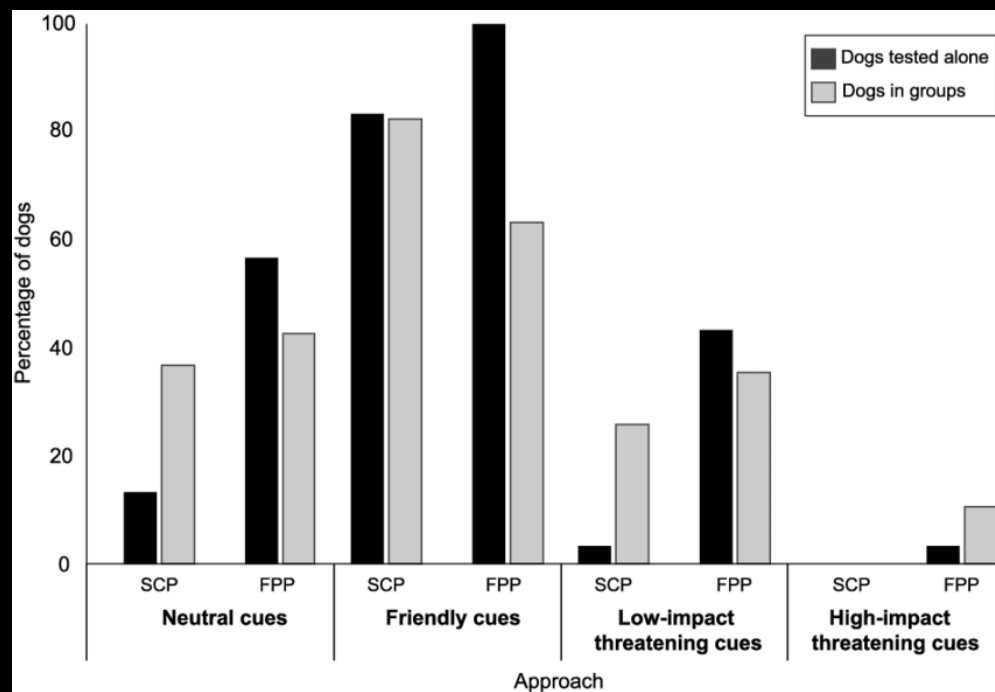


~ 0.8

Let's play a game...

Is this a graph about dogs?

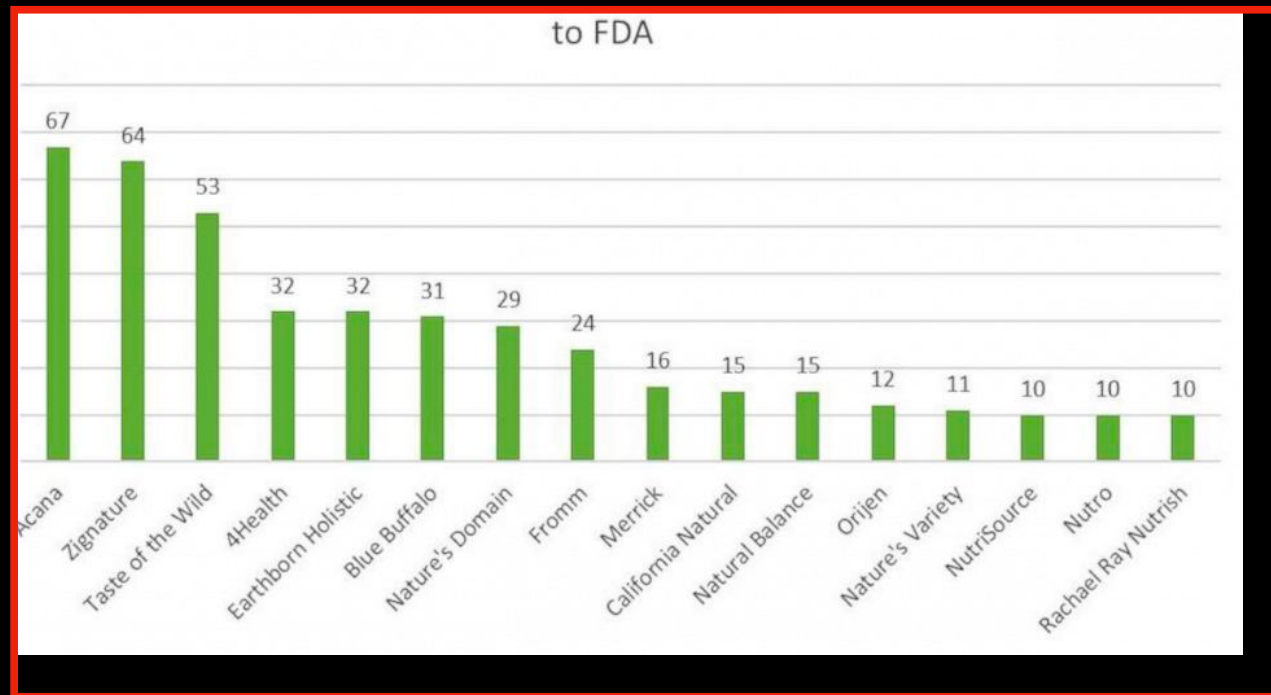
Raise your hand if you see a *graph* about dogs (anything at all to do with dogs):



DO NOT raise your hand if the image is not a graph about dogs.

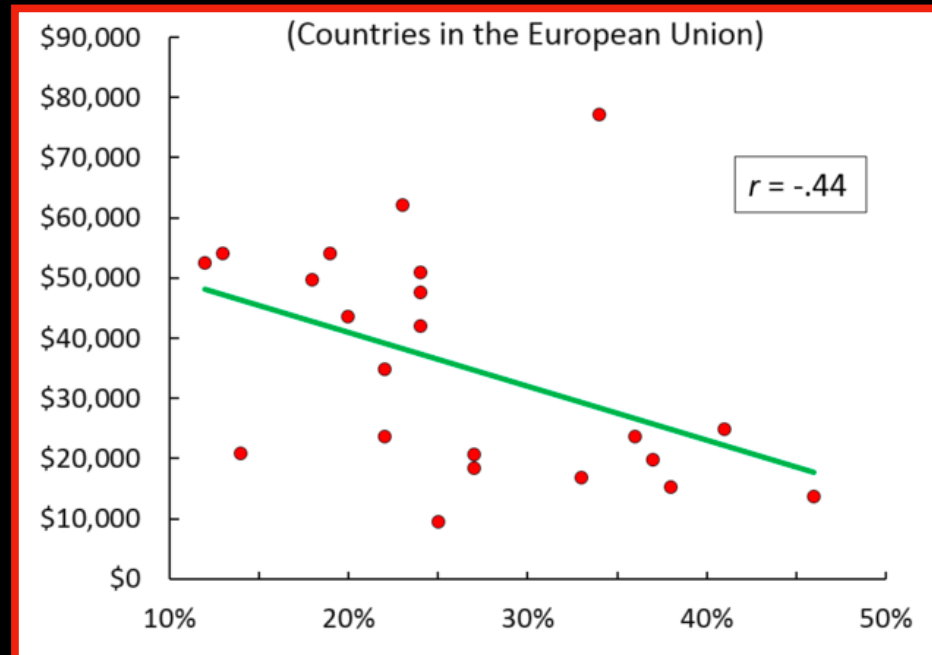
Let's play a game...

Raise your hand if this is graph about dogs



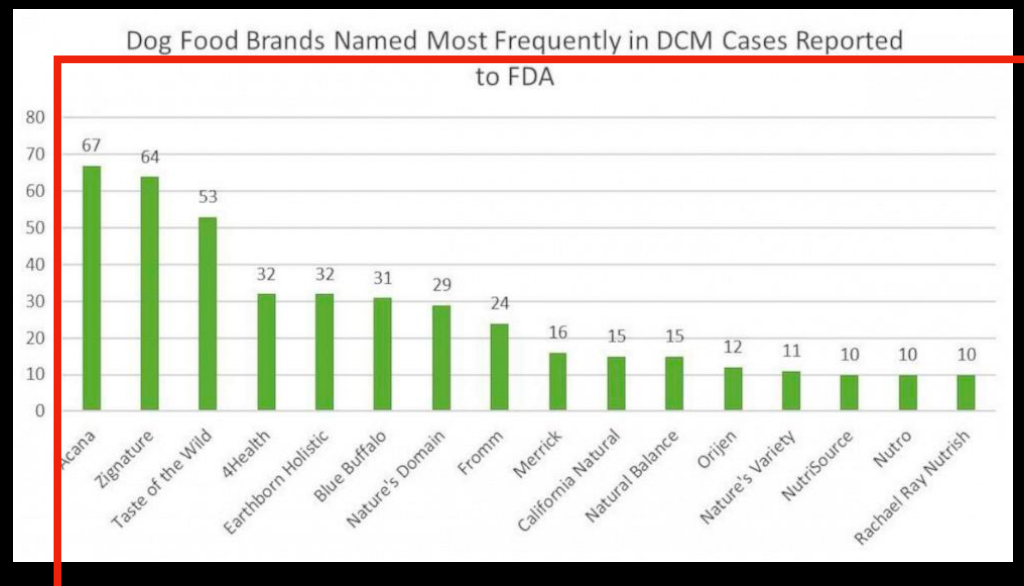
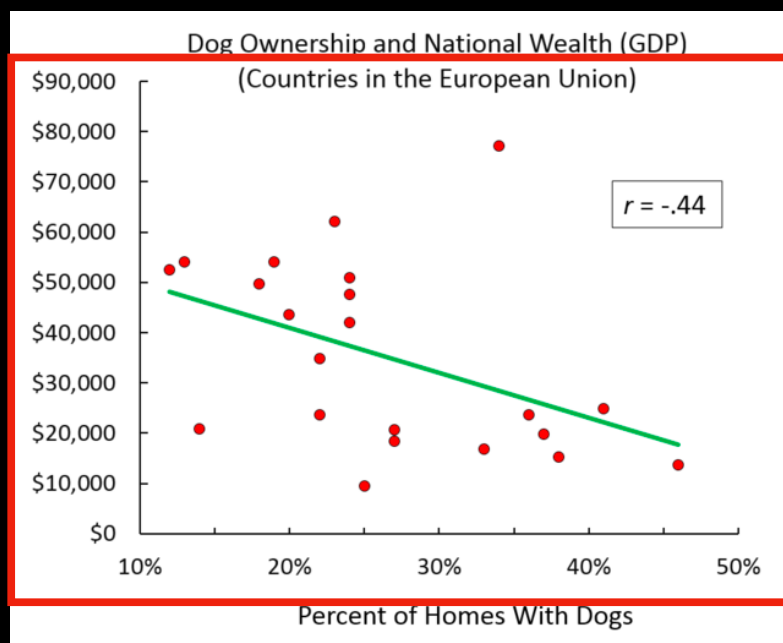
Let's play a game...

Raise your hand if this is graph about dogs



Let's play a game...

Raise your hand if this is graph about dogs



They are both graphs about dogs!

What did we notice about the differences between Version #1 and Version #2?